ACS APPLIED MATERIALS & INTERFACES

Research Article

www.acsami.org

Oxygen Sensitivity of Atomically Passivated CdS Nanocrystal Films

Lorenzo Maserati,[†,‡] Iwan Moreels,[†] Mirko Prato,[†] Roman Krahne,[†] Liberato Manna,[†] and Yang Zhang*[,†]

[†]Istituto Italiano di Tecnologia, Via Morego 30, 16163 Genova, Italy

[‡]Department of Physics, University of Genoa, Dodecaneso 33, 16146 Genova, Italy

Supporting Information

ABSTRACT: CdS nanocrystals (NCs) synthesized by colloidal chemistry methods have been intensively studied for various applications. However, little attention has been paid to the interaction between the oxygen molecules present in air and the NC surface, which has a strong influence on the electrical properties of NC films. Here, we discuss the effect of oxygen adsorption at the NC surface on the photoconductivity of CdS NC films that were treated by propyltrichlorosilane, which is known to replace the native ligands at the NC surface with chloride ions. The photocurrent−voltage (PIV) characteristics of NC@Cl films recorded under oxygen atmosphere reveal a significant reduction in the photocurrent, as compared to those recorded under argon or vacuum. We demonstrate that this reduction can be related to adsorbed oxygen ions that effectively passivate the NC surface. This passivation reduces the free electron concentration and thereby reduces the photocurrent. Furthermore, we have investigated the light intensity dependence of the photocurrent dynamics of our devices in argon and in oxygen. These measurements confirm that the adsorption of oxygen is a photo-assisted process. Eventually, the potential of using our devices as oxygen sensors is assessed. A remarkable sensitivity of 35 is obtained at room temperature for 10% (concentration) oxygen flow, which is at least one order of magnitude higher than the results reported in the literature. Our work clarifies the mechanism of the photoconductivity reduction in CdS NC films upon oxygen adsorption and opens up opportunities of exploring such devices for gas sensing applications.

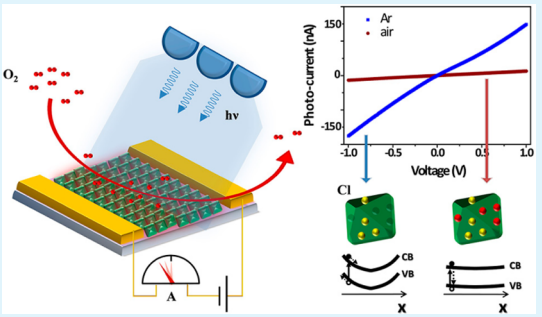

KEYWORDS: *CdS nanocrystal films, photoconductivity, oxygen adsorption, surface passivation, oxygen sensing*

1. INTRODUCTION

Colloidal nanocrystals (NCs) have been intensively developed in the past decades and applications in many technological fields have been proposed.[1] Colloidal NCs, due to their synthesis methods, are in most cases coated with a layer of organic molecules that guarantees their stability in various solvents.[2] However, these stabilizing molecules are typically of long aliphatic chains, which can efficiently inhibit charge hopping from NC to NC in a film, making films of surfactant passivated NCs poorly conducting. Recently, several procedures have been developed to replace the native ligands at the surface of colloidal NCs with smaller molecules and clusters, down to single atoms/ions, and these treatments have translated into much improved electrical conductivity,[3−5] since the inter-NC spacing is considerably reduced. An additional advantage of replacing bulky ligands with smaller passivating agents is that the surface of NCs should become more accessible to external agents, such as gaseous species. This would potentially translate into an increased sensitivity of the electronic and electrical transport properties of NC films to the external environment, which can be exploited in gas sensing applications (a research in which the use of NCs is under constant scrutiny).[6−8]

In this work, we report the influence of surface oxygen adsorption on the photoconductivity of films made of CdS NCs passivated with chloride ions. We choose CdS NCs as a sensing material and oxygen as a target gas because the influence of oxygen adsorption on the photocurrent of bulk CdS and macroscopic size CdS platelets with several micrometers in diameter has been discussed in various works.[9−11] On the other hand, little has been reported on the impact of oxygen adsorption on the photoconductive behavior of films of CdS NCs, and higher sensitivity is expected from sensors based on NC films with respect to bulk CdS or micrometer size CdS particle films, because of the increased surface to volume ratio in NCs.[12−14] Also, we chose to passivate the surface of NCs with chloride ions, following a ligand exchange procedure first reported by Owen et al. on CdSe NCs.[15] We recently adapted and extended this procedure to films of NCs of various materials,[16] because this kind of atomic passivation was proven to improve the conductivity of NC films by several orders of magnitude with respect to films of the same NCs coated by the native surfactant ligands.[3,17]

The oxygen adsorption had a remarkable impact on the electrical and optical properties of our CdS@Cl NC films. In the presence of oxygen, the photocurrent−voltage characteristics showed a significant quenching of the photocurrent, while

Received: March 28, 2014
Accepted: May 6, 2014
Published: May 6, 2014

both the band-to-band emission and the emission from trap states were enhanced by 100% and 64%, respectively. We rationalized such behavior according to the following model: we assume that the surface states of the NCs, which resulted from the incomplete Cl^- passivation[18] and which were probed by photoluminescence (PL) measurements, led to a built-in electric field near the NC surface that contributed to the electron-hole dissociation under Ar atmosphere or vacuum.[19] Their passivation with oxygen atoms (probably through a charge-transfer bond[20]) resulted in a decrease of the built-in electric field, and thus increased the recombination rate of the photo-generated electron-pairs and consequently the light emission. Meanwhile, the increase of the recombination rate diminished the concentration of free charge carriers in the film, resulting in lower photoconductivity. Time traces of the photocurrent under Ar and O_2, recorded while switching the illumination on and off, evidenced that the oxygen adsorption on the NC surface was a photo-assisted process. We then tested the sensing performance of our thin film devices towards oxygen at room temperature, and determined a sensitivity (defined as the relative change of the device resistance with respect to the initial resistance) of 35 in 10% oxygen flow. This sensitivity is higher than that reported in previous works.[21−24]

2. EXPERIMENTAL SECTION

NC Film Deposition and Film Treatment. The relatively large (~18 nm in diameter) CdS NCs studied in this work were synthesized following a seeded-growth approach: first, small CdS seeds were synthesized by a procedure similar to the one reported by Carbone et al.,[25] with minor modifications (we used tri-n-octyl phosphine sulfide as the sulfur source). Next, a thick shell was grown on them at 300 °C by adding the Cd- and S- precursors drop-wise over 4 h,[26] to avoid homogeneous nucleation of small CdS clusters. SiO_2/Si substrates were patterned with Ti/Au (thickness 5/100 nm) interdigitated electrodes by direct laser writing on SU8 resist, electron-beam evaporation of metals, and followed by a lift-off process in a Remover PG solution. The patterned substrates were cleaned with a standard cleaning procedure (immersion in acetone, isopropanol, deionized water) and were then irradiated with UV light for 2 min prior to NC deposition to increase the philicity of the substrate surface to toluene. The NCs were deposited from a toluene solution via the layer-by-layer (lbl) deposition technique onto substrates as follows (similarly to our previously reported work[16]): a toluene drop of 15 μL with a NC concentration of ~1.5 μM was deposited on a SiO_2/Si substrate (dimension 7 × 7 mm^2). The substrate was immediately spun at 2000 rpm for 60 seconds to spread the drop evenly and allow the toluene to evaporate. The ligand exchange process was done by dipping the substrate in a propyltrichlorosilane (PTCS) solution (0.1 M PTCS in acetonitrile) for 10 min, followed by rinsing in acetonitrile, and drying in the glovebox. The sample was rinsed in toluene in order to remove possible organic residuals, and after drying, the sample was positioned back on the spin coater and the above-described procedure was repeated 3 times to achieve about a 100 nm thick NC film. The film homogeneity was evaluated by a scanning electron microscope at different magnifications, spanning nanometer to centimeter scale (see Figure S1 of the Supporting Information (SI) for details).

Transmission Electron Microscopy (TEM) Analysis. For TEM, the samples were prepared by drop-casting the NC solution on carbon-coated 200-mesh copper grids, and the images were acquired with a JEOL JEM-1011 microscope operating at an accelerating voltage of 100 kV.

Scanning Electron Microscopy (SEM). SEM images were obtained by a JEOL JSM 7500FA microscope operating at 15 kV.

Photoluminescence Spectra. PL spectra were collected with an Edinburgh Instruments FLS920 spectrofluorometer, exciting the films at a wavelength of 400 nm.

Electrical Measurements in Controlled Atmospheres. Interdigitated electrodes with a spacing of 5 μm were used. The electrodes were contacted by wire-bonding to an electrical socket that could be fitted into a glass flask (gas chamber) in which the gases were flushed. The Ar and O_2 used in our experiments were of high purity (≥99.999%). The gas flow was regulated by mass flow controllers (MFCs) and an electrical valve mounted on a rotary pump that could evacuate the chamber from gases (see Scheme 1). The pressure inside the gas chamber was monitored by a downstream gauge; a pressure of ~1 mTorr could be achieved with the downstream pump fully running and MFCs being closed. The illumination was provided by four blue InGaN light emitting diodes (LED) outside the flask that peaked at 467 nm with a full width at half maximum (FWHM) of 30 nm. The light intensity could be tuned from 0 to 20 mW/cm^2 by changing the applied voltage bias on LEDs with a power source (Keithley 2200-60-2). The electrical characterization of the NC films was performed with a Keithley sourcemeter (Keithley 2612), configured in the source-voltage-read-current mode. All measurements were performed at a pressure of 740 Torr inside the gas chamber except for the measurement in vacuum (~1 mTorr). Prior to all measurements, the samples were kept under stable conditions for 10 min and allowed to achieve equilibrium in different atmospheres. For example, if measurements were to be carried out in the dark (or under 20 mW/cm^2 illumination), we placed the sample in the dark (or under 20 mW/cm^2 illumination) for 10 min before starting to record the current; similarly, while changing atmosphere (e.g., from Ar to O_2), three purging (evacuating-refilling) cycles were performed prior to the measurements, which ensured evacuation of the previous gas from the chamber.

Scheme 1. Experimental Setup for Measuring the Photoconductivity of CdS NC Films under Controlled Atmosphere (e.g., O_2, Ar)[a]

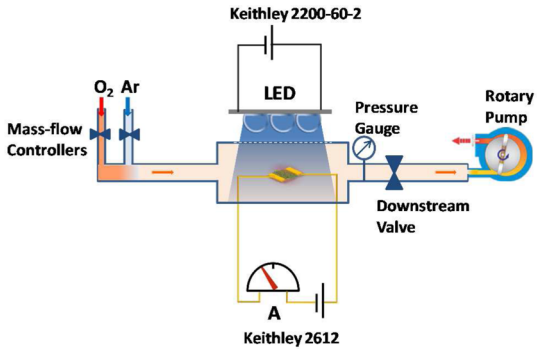

[a]See main text for a detailed description of the setup.

3. RESULTS AND DISCUSSION

Figure 1a shows a TEM image of the CdS NCs. They had a wurtzite crystal structure, as assessed by X-ray diffraction (XRD) analysis (see Figure S2 of the SI). The average size of the NCs extracted from the TEM data analysis was 18 nm, with a size dispersion of 2 nm (standard deviation). The estimated surface-to-volume (S/V) ratio of these nanocrystals is about 2.5 × 10^8 m^{-1}, which translates into an overall S/V ratio increase in the NC film of ~3 orders of magnitude with respect to a typical bulk CdS film (see SI for the estimates of S/V ratios).[27] We chose to use these relatively large NCs to construct our devices because we found that the PTCS treatment tends to work better on CdS NCs with larger diameter (>10 nm) than on the smaller ones. Figure 1b shows a typical SEM image of CdS NC films fabricated via the process described in section 2. A good film uniformity across large areas (~centimeter scale) was

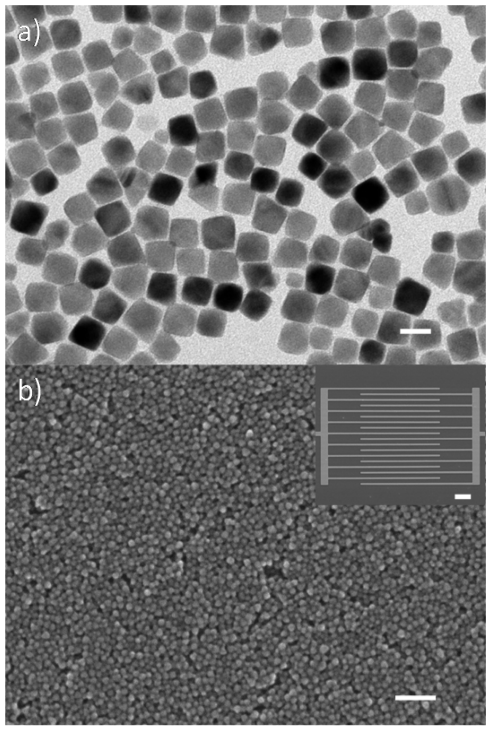

Figure 1. (a) TEM image of CdS NCs. (b) High resolution SEM image of a film deposited on a SiO_2/Si substrate and treated with PTCS. The inset is a SEM image of a 5 μm spaced interdigitated electrodes structure. Scale bars represent (a) 20 nm; (b) 100 nm (inset 20 μm).

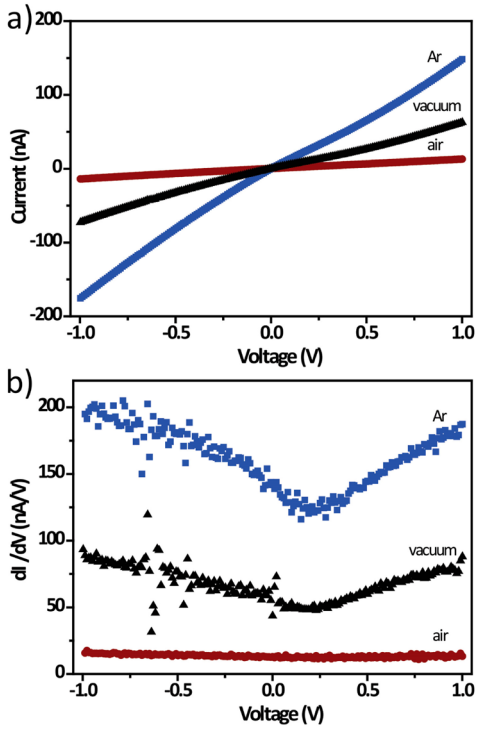

Figure 2. (a) Photocurrent versus voltage characteristics of devices exposed to air (dark red), kept under Ar (blue), and in vacuum (black). (b) Differential conductance as a function of voltage bias derived numerically from part a.

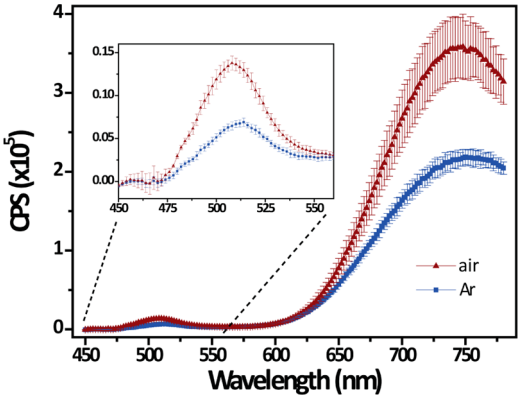

Figure 3. Photoluminescence spectra of a CdS NC film under Ar (blue squares) and in air (dark red triangles). A vial was used to house the sample and maintain the atmosphere surrounding it. Three consecutive cycles of Ar-to-air measurements have been performed. The reported data was averaged and the error bars were plotted to indicate the deviation of the measurement from cycle to cycle. The inset shows the spectra from 450 to 560 nm on an enlarged scale.

achieved by the lbl spin-coating of NCs on SiO_2/Si substrates from a toluene solution. The PTCS treatment, on the other hand, significantly improved the photoconductivity in these films by removing the long-chain capping ligands (e.g., trioctylphosphine oxide and alkylphosphonic acids) and leaving the surface partially passivated by Cl atoms.[16] The inset in Figure 1b shows a SEM image of the interdigitated electrodes used for the electrical measurements in this work.

The photocurrent−voltage (PIV) characteristics of the CdS NC films, when exposed to different gas atmospheres (Ar and air) or to vacuum are reported in Figure 2a. The photocurrent was reduced significantly (by orders of magnitude) in the presence of oxygen with respect to Ar and vacuum, in agreement with the results reported on bulk CdS films in the literature.[5−7,19] The lower photocurrent under vacuum (1 mTorr) with respect to Ar could result from residual oxygen content in the chamber, since the oxygen concentration in the chamber after three purging cycles with Ar was likely lower than that at a pressure of ∼1 mTorr. Apart from the large difference in current amplitude, we observed a more linear PIV curve in air with respect to those recorded in vacuum and in Ar. This difference can be readily seen in Figure 2b, which plots the differential conductance derived from Figure 2a as a function of the applied voltage bias. The differential conductance in vacuum (black) and Ar (blue) rises with increasing applied voltage bias, while the one in air (dark red) is approximately constant over the applied voltage bias range.

The PL spectra of a CdS NC film recorded at room temperature under Ar and in air are presented in Figure 3. The spectra show two emission bands centered at 508 and 748 nm that can be assigned to the band-edge and surface-trap-states emission, respectively.[28] The PL spectra reveal two interesting features: First, the emission from the trap states is much stronger than the band-to-band emission, which is evident both in Ar and in air. This disparity in emission indicates that the majority of photo-generated electrons relaxes to trap states within the bandgap prior to recombination. More importantly, we observed that the emission from surface trap states and inter-band recombination were enhanced by 64% and 100%, respectively, when exposing the sample to air (see the dark red curve in Figure 3 and its inset). This enhancement points to the fact that the radiative recombination rate inside the NCs increased when oxygen molecules adsorbed on the NC surface.

dx.doi.org/10.1021/am501906y | ACS Appl. Mater. Interfaces 2014, 6, 9517−9523

We have neglected the effect of the moisture in the air in our discussion due to its small partial pressure compared to oxygen and to the qualitatively similar behavior that we observed on photocurrents measured under air and pure oxygen atmosphere (see Figure S3 of the SI). Generally speaking, moisture can be expected to give rise to hysteresis in the PIV curves as it was reported for CdS films,[27] which, however, we did not observe in our experiments.

We adopt a simple model that describes the effect of the surface states on the energy bands of the NCs.[19] First, we can assume that surface states are associated with unpassivated Cd^{2+} atoms or with sulfur vacancies at the surface, which create energy levels ~0.7 eV below the bottom of the conduction band.[29−31] Assuming that the Fermi level of such surface states lies below the one of the CdS NC itself, they give rise to the surface-state-induced upward band bending after equilibration (due to the transfer of electrons from the NC bulk to the positively charged surface states),[19] as shown in Figure 4a.

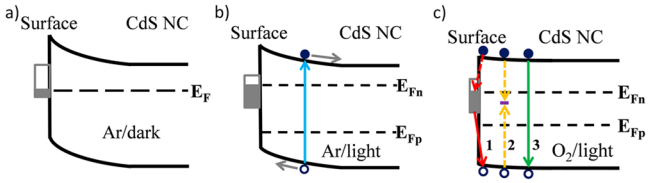

Figure 4. Electronic energy band diagram of a single CdS NC (in steady state) under Ar atmosphere and in dark (a), and with above-bandgap light illumination in Ar (b) and in O_2 (c). E_F and $E_{Fn(p)}$ are the Fermi level in equilibrium and the quasi-Fermi level of electrons (holes) under illumination, respectively. In panel a, the Fermi level is pinned to the surface states, while the Fermi levels in panels b and c become unpinned due to light illumination.[41] Gray rectangles on the surface represent the surface states, which are most likely created by the unpassivated Cd atoms. These states are partially filled according to the height of the (quasi-)Fermi level. The defect levels that serve as recombination centers are represented by a short purple line in panel c. The smaller gray rectangle in panel c exemplifies the decrease of the number of surface states when the surface is passivated with negative oxygen ions. The light blue arrow in panel b indicates the optical transition of electrons from valence band to conduction band upon absorption of photons. The filled (empty) blue circles denote the photo-excited electrons (holes). Gray arrows indicate the dissociation of excitons after generation by the built-in electric field near the surface. The arrows in panel c indicate three possible channels for the recombination of electron-hole pairs: (1) recombination from surface trap states to the valence band (red); (2) Shockley−Read−Hall recombination (dashed yellow);[42] (3) inter-band recombination (green).

When above-bandgap light illuminates the NC, electron-hole pairs are generated (shown as filled and empty circles in Figure 4b). A large fraction of these electron-hole pairs are dissociated by the built-in electric field to create free electrons and holes, while others recombine again after generation. When electron-hole pairs are separated, holes travel towards the surface and recombine with the trapped electrons via surface recombination. On the other hand, free electrons would either remain in the conduction band and contribute to the photocurrent flow (in the presence of an external electric field) or would be captured by the surface trap states resulting in filling of the gap states (denoted by the solid gray rectangle in Figure 4b).

In the following, we discuss the effect of oxygen adsorption. Oxygen is known to adsorb on the surface of many semiconductors.[32−35] In the dark, oxygen molecules would mainly adsorb physically on the surface of CdS NCs due to the lack of free electrons in these NCs. However, in the presence of light (and hence photo-generated free electrons), Mark et al. and other authors suggested that oxygen, owing to its high electronegativity, would chemisorb (i.e., form a charge-transfer bond[20]) on the surface of CdS NCs as negatively charged ions, by taking electrons from surface states or from the conduction band of CdS.[9,10,20,36] In particular, negative oxygen ions that form charge-transfer bonds[20] with Cd^{2+} ions would effectively passivate the surface dangling bonds of Cd atoms that were left unpassivated after the PTCS treatment,[16] decreasing the number of surface states. On the other hand, the extent of band bending is positively correlated with the amount of electrons transferred from the NC bulk to the surface states. Since the number of surface states is decreased due to oxygen passivation, it is reasonable to assume that the number of electrons transferred is also diminished, and thus, the upward bending of the energy band (induced by the filling of surface states[19]) will be reduced to form a nearly flat band, as displayed in Figure 4c. Along with the flattening of the energy band, the built-in electric field near the surface would vanish. This will bring, as a consequence, a significant increase in the recombination rate of the electron-hole pairs, due to the lack of an internal electric field to dissociate these pairs immediately after the generation. This increase can account for the enhancement in the light emission and also is most likely responsible for the reduction in the efficiency of free carrier generation (which is the number of free carriers produced by one absorbed photon) in the NCs. Since the free carrier concentration is abated, it follows that the photocurrent decreases, and this is corroborated by our experimental results shown in Figure 2a.

We are additionally able to provide a plausible explanation for the change from nonlinear PIV curves with higher absolute photocurrent under Ar or vacuum to almost linear behavior with lower photocurrent under O_2 atmosphere. The difference in photocurrent magnitude can be related to the more efficient exciton dissociation due to the built-in field, as discussed above. Once dissociated, the free charges can contribute to the photocurrent via two channels:[37] hopping transport via surface trap states, and/or core to core charge transport via direct tunneling through the barriers between neighboring NCs. For the atomically passivated NCs (i.e. after PTCS treatment) the width of the tunnel barriers between individual NCs should be very small, since this is characterized by an atomic layer passivating the surface. If the barrier height is much larger than the voltage drop per NC caused by the applied bias (i.e., the voltage drop has no effect on the effective tunnel barrier), then this channel will yield linear PIV behavior.[38,39] On the other hand, trap state mediated charge transport very often results in nonlinear characteristics,[37,40] and this channel is largely suppressed under oxygen due to effective passivation of the surface states, while it has dominant contribution under Ar and vacuum.

To further examine the process of oxygen adsorption/desorption, we investigated the photocurrent dynamics of our devices at different light intensities. Panels a and b of Figure 5 show the results obtained in Ar and in O_2, respectively. Note that, prior to all these experiments, the chamber was purged by dry gases (i.e., Ar or O_2) for three times. Therefore, we expect that the effect of the water adsorbed at the NC surface on the film conductivity can be neglected. It is obvious that the photocurrent increases with increasing light intensity in all

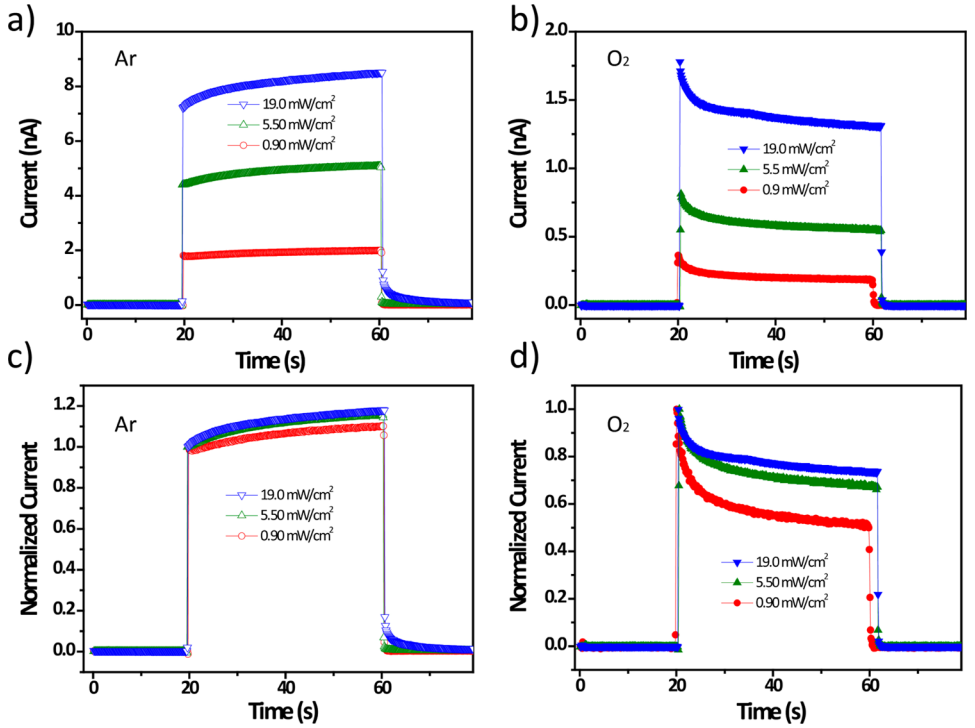

Figure 5. Dynamics of photocurrent recorded in Ar (a and c) and in O_2 (b and d) at different light intensities at a fixed voltage bias of 1 V. The LEDs (see Experimental Section) were turned on at t = 20 s and turned off at t = 60 s. Photocurrent time traces in panels a and b are normalized with respect to the values at t = 20 s, and the results of the normalization are presented in parts c and d, respectively.

cases, with an initial rise time that is faster than the time interval of 50 ms per data point that we set for the measurement. In addition, one can easily see that the time traces of photocurrent measured in Ar and in O_2 exhibit two distinct patterns for all light intensities, as described in the following.

(I) Time traces under Ar: Here, the current (Figure 5a) increases abruptly to a certain level (depending on the light intensity and the voltage bias) once light from the LEDs is turned on, and then continues to increase asymptotically to a saturation level on a time scale of minutes. This gradual increase of the photocurrent might be ascribed to the slow desorption of the previously adsorbed oxygen molecules on the surface of the NCs by photo-generated holes (see Figure S4 of SI for the XPS data on our NC films).[9,10] After electron-hole pair generation, holes would travel to the surface of NCs. A fraction of the holes recombine with the trapped electrons via surface recombination, and the others neutralize the negatively charged oxygen species adsorbed on the surface, releasing them to the surrounding environment. The re-adsorption of oxygen (which reduces the photocurrent) occurs in parallel in the presence of photo-generated electrons, which, along with the desorption, eventually brings on a steady-state photocurrent (see Figure S5 of SI for the saturated photocurrent at prolonged time scales). In addition, the trapping and de-trapping of free carriers associated with surface trap states might also play a role in the evolution of the photocurrent into a steady level.

(II) Time traces under O_2: Here, the current (Figure 5b) also rises abruptly upon illumination, but then decays to a steady level in the following minutes. The decay of the photocurrent with time closely follows a logarithmic behavior (see Figure S6 of SI for the fit to the curve) that can be related to the Elovich equation, which describes the kinetics of the adsorption of gas species on semiconductor surfaces involving electron transfer.[43,44] This logarithmic decay gives evidence of the photo-assisted adsorption of oxygen. Steady state is reached on a time scale of minutes by the decrease of the number of available adsorption sites with increasing oxygen accumulation at the NC surface, together with the simultaneous desorption of oxygen.

To illustrate the effect of light intensity on the photocurrent dynamics, we normalize the photocurrent curves with respect to their values at light turn-on. Figure 5c shows that the light intensity has little effect on the rate of the photocurrent increase when the sample is under Ar, which is evidenced by the small differences between the curves. However, when the sample is under O_2, the light intensity plays an important role in determining the photocurrent evolution, which is demonstrated by the significant dispersion of the normalized photocurrent time traces in Figure 5d. Note that the decay is more pronounced at low light intensities. Interestingly, we notice that a stable photocurrent can be achieved in seconds through the simultaneous control of the oxygen concentration and the light intensity (see the green curve in Figure S4 of SI).

To explore our NC films for gas sensing applications, we performed one-cycle sensing measurements of oxygen in an air-tight gas chamber at room temperature. The measurement consisted of three consecutive steps: (1) baseline recording in Ar; (2) response to O_2; (3) recovering in Ar. The results are shown in Figure 6 where two different concentrations (1% and 10%) of oxygen diluted in Ar were used. The sensitivity (S) of the device is defined by[14,45]

dx.doi.org/10.1021/am501906y | ACS Appl. Mater. Interfaces 2014, 6, 9517−9523

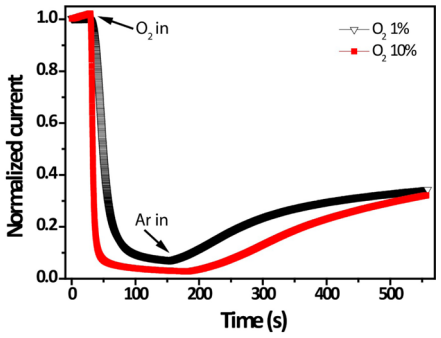

Figure 6. One-cycle gas sensing experiment toward two concentrations (1% and 10%) of oxygen. The device was biased at 1 V, and illuminated with blue LEDs at an intensity of 20 mW/cm^2. A flow of diluted oxygen was allowed to enter the gas chamber at t = 40 s (indicated by the upper arrow), and was cut off at t = ∼180 s. Pure Ar was re-introduced to the gas chamber at t = ∼180 s (indicated by the lower arrow) to recover the device.

$$S = \frac{R_{O_2} - R_{Ar}}{R_{Ar}} \quad (1)$$

where R_{Ar} is the initial resistance of the sensing device in Ar, and R_{O_2} is the resistance of the sensing device under O_2 for a certain period of time (here ∼150 s).

The sensitivities calculated from the curves in Figure 6 are ∼13 and ∼35 for oxygen concentrations of 1% and 10%, respectively. These room temperature sensitivity values are superior to those reported in other works,[21−24] thanks to the large S/V ratio associated with our NCs and the effective removal of the native ligands at the NC surface (see Figure S7 of SI for a comparison with a sample passivated by native ligands). For example, Neri et al. reported a sensitivity of ∼0.5 for an oxygen concentration of 10% with platinum-doped In_2O_3 nanocrystals as sensing materials.[22] Moreover, the sensitivity might be further improved by illuminating the devices at much lower light intensities (e.g., 1 mW/cm^2), as lower light intensity generally gives larger relative quenching of the photocurrent (shown in Figure 5d). In addition, we observe a relatively fast response time (defined as the time it takes for the sensor to reach 63.2% of the overall resistance change, i.e., the time constant of the dynamic response of a first-order system) of ∼4.5 s for 10% oxygen concentration, as compared to recently developed gas sensors.[46] This response time represents an upper limit because it also depends on the time needed to stabilize the targeted O_2 concentration in the gas chamber. We note that the recovery of our devices in Ar was slow, likely due to the low efficiency of the desorption of oxygen from the NC surface. The recovery should be accelerated by heating up the film[46] or by flowing a high density of current through the film.[47] Nevertheless, the high oxygen sensitivity of our devices makes films of CdS NCs treated with PTCS interesting for oxygen detectors operating at ambient temperatures.

4. CONCLUSIONS

The exposed surface of CdS NC films passivated with chloride ions makes their photoconductive behavior strongly sensitive to their environment. Oxygen reduces significantly the photoconductivity due to effective surface passivation, while under Ar and vacuum unpassivated surface states lead to more effective charge separation of the photo-generated electron−hole pairs and additional conductive channels, thus increasing the photocurrent. We rationalized this behavior in terms of energy band bending at the NC surface that critically depends on the filling and passivation of surface trap states. This rationale should apply to large variety of NC materials, provided that they are passivated by atomic ligands, and therefore will contribute to the general understanding of conductivity in these recently developed NC solids.

■ ASSOCIATED CONTENT

Supporting Information

(1) SEM images of spin-coated CdS NC films on the scales from nanometer to millimeter, (2) XRD pattern of the CdS NCs, (3) estimates of the surface-to-volume ratios, (4) stabilized photocurrent plotted as a function of oxygen concentration, (5) XPS spectra of CdS NCs films capped with the native ligand and passivated with chloride ions, (6) photocurrent variation over time due to light switching for different oxygen concentrations, (7) fit to the photocurrent decay in O_2 using Elovich equation when light was turned on, and (8) comparison of photocurrent response to CdS NCs capped by native ligands and treated with PTCS solution. This material is available free of charge via the Internet at http://pubs.acs.org

■ AUTHOR INFORMATION

Corresponding Author

*Email: yangzh08@gmail.com.

Notes

The authors declare no competing financial interest.

■ ACKNOWLEDGMENTS

The authors thank F. De Donato for providing the CdS NC samples, A. Scarpellini for support in SEM imaging, and S. Marras for assistance in XRD analysis. The research leading to these results has received funding from the European Union's Seventh Framework Program (FP7/2007-2013) under grant agreement No. 298022 (NIRPLANA, I.M.) and No. 614897 (TRANS-NANO, L.M.)

■ REFERENCES

(1) Talapin, D. V.; Lee, J. S.; Kovalenko, M. V.; Shevchenko, E. V. Prospects of Colloidal Nanocrystals for Electronic and Optoelectronic Applications. *Chem. Rev.* **2010**, *110*, 389−458.

(2) Yin, Y.; Alivisatos, A. P. Colloidal Nanocrystal Synthesis and the Organic−Inorganic Interface. *Nature* **2005**, *437*, 664−670.

(3) Lee, J. S.; Kovalenko, M. V.; Huang, J.; Chung, D. S.; Talapin, D. V. Band-like Transport, High Electron Mobility, and High Photoconductivity in All-Inorganic Nanocrystal Arrays. *Nat. Nanotechnol.* **2011**, *6*, 348−352.

(4) Tang, J.; Kemp, K. W.; Hoogland, S.; Jeong, K. S.; Liu, H.; Levina, L.; Furukawa, M.; Wang, X. H.; Debnath, R.; Cha, D. K.; Chou, K. W.; Fischer, A.; Amassian, A.; Asbury, J. B.; Sargent, E. H. Colloidal-Quantum-Dot Photovoltaics Using Atomic-Ligand Passivation. *Nat. Mater.* **2011**, *10*, 765−771.

(5) Webber, D. H.; Brutchey, R. L. Ligand Exchange on Colloidal CdSe Nanocrystals Using Thermally Labile tert-Butylthiol for Improved Photocurrent in Nanocrystal Films. *J. Am. Chem. Soc.* **2011**, *134*, 1085−1092.

(6) Pick Chung, L.; Robert, A. N.; Masud, M.; Nasser, P. An Effective and Simple Oxygen Nanosensor Made from MPA-Capped Water Soluble CdTe Nanocrystals. *Nanotechnology* **2013**, *24*, 015501.

(7) Neri, G.; Bonavita, A.; Micali, G.; Rizzo, G.; Galvagno, S.; Niederberger, M.; Pinna, N. A Highly Sensitive Oxygen Sensor

Operating at Room Temperature Based on Platinum-Doped In_2O_3 Nanocrystals. *Chem. Commun.* **2005**, 6032−6034.
(8) Liu, H.; Li, M.; Voznyy, O.; Hu, L.; Fu, Q.; Zhou, D.; Xia, Z.; Sargent, E. H.; Tang, J. Physically Flexible, Rapid-Response Gas Sensor Based on Colloidal Quantum Dot Solids. *Adv. Mater.* **2014**, DOI: 10.1002/adma.201304366.
(9) Mark, P. Photo-Induced Chemisorption on Insulating CdS Crystals. *J. Phys. Chem. Solids* **1964**, *25*, 911−920.
(10) Weber, E.-h. Surface Photoconductivity of CdS Influenced by Chemisorption and Desorption of Oxygen. *Phys. Status Solidi B* **1968**, *28*, 649−662.
(11) Bube, R. H. The Basic Significance of Oxygen Chemisorption on the Photoelectronic Properties of CdS and CdSe. *J. Electrochem. Soc.* **1966**, *113*, 793−798.
(12) George, C.; Dorfs, D.; Bertoni, G.; Falqui, A.; Genovese, A.; Pellegrino, T.; Roig, A.; Quarta, A.; Comparelli, R.; Curri, M. L.; Cingolani, R.; Manna, L. A Cast-Mold Approach to Iron Oxide and Pt/Iron Oxide Nanocontainers and Nanoparticles with a Reactive Concave Surface. *J. Am. Chem. Soc.* **2011**, *133*, 2205−2217.
(13) Krahne, R.; Morello, G.; Figuerola, A.; George, C.; Deka, S.; Manna, L. Physical Properties of Elongated Inorganic Nanoparticles. *Phys. Rep.* **2011**, *501*, 75−221.
(14) Zhang, Y.; Cui, S.; Chang, J.; Ocola, L. E.; Chen, J. Highly Sensitive Room Temperature Carbon Monoxide Detection Using SnO_2 Nanoparticle-Decorated Semiconducting Single-Walled Carbon Nanotubes. *Nanotechnology* **2013**, *24*, 025503−025503.
(15) Owen, J. S.; Park, J.; Trudeau, P. E.; Alivisatos, A. P. Reaction Chemistry and Ligand Exchange at Cadmium−Selenide Nanocrystal Surfaces. *J. Am. Chem. Soc.* **2008**, *130*, 12279−12281.
(16) Zanella, M.; Maserati, L.; Pernia Leal, M.; Prato, M.; Lavieville, R.; Povia, M.; Krahne, R.; Manna, L. Atomic Ligand Passivation of Colloidal Nanocrystal Films via their Reaction with Propyltrichlorosilane. *Chem. Mater.* **2013**, *25*, 1423−1429.
(17) Kovalenko, M. V.; Scheele, M.; Talapin, D. V. Colloidal Nanocrystals with Molecular Metal Chalcogenide Surface Ligands. *Science* **2009**, *324*, 1417−1420.
(18) Wang, Y.; Zhang, Y.; Zhang, W. First-Principles Study of the Halide-Passivation Effects on the Electronic Structures of CdSe Quantum Dots. *RSC Adv.* **2014**, DOI: 10.1039/c4ra01268b.
(19) Zhang, Z.; Yates, J. T. Band Bending in Semiconductors: Chemical and Physical Consequences at Surfaces and Interfaces. *Chem. Rev.* **2012**, *112*, 5520−5551.
(20) Vempati, S.; Ertas, Y.; Uyar, T. Sensitive Surface States and their Passivation Mechanism in CdS Quantum Dots. *J. Phys. Chem. C* **2013**, *117*, 21609−21618.
(21) Afify, H. H.; Battisha, I. K. Oxygen Interaction with CdS Based Gas Sensors by Varying Different Preparation Parameters. *J. Mater. Sci.: Mater. Electron.* **2000**, *11*, 373−377.
(22) Neri, G.; Bonavita, A.; Micali, G.; Rizzo, G.; Galvagno, S.; Niederberger, M.; Pinna, N. A Highly Sensitive Oxygen Sensor Operating at Room Temperature Based on Platinum-Doped In_2O_3 Nanocrystals. *Chem. Commun.* **2005**, 6032−6034.
(23) Smyntyna, V.; Gerasutenko, V.; Golovanov, V.; Kačiulis, S.; Mattogno, G.; Viticoli, S. Surface Spectroscopy Study of CdSe and CdS Thin-Film Oxygen Sensors. *Sens. Actuators, B* **1994**, *22*, 189−194.
(24) Zuruzi, A. S.; Kolmakov, a.; MacDonald, N. C.; Moskovits, M. Highly Sensitive Gas Sensor Based on Integrated Titania Nanosponge Arrays. *Appl. Phys. Lett.* **2006**, *88*, 102904.
(25) Carbone, L.; Nobile, C.; De Giorgi, M.; Sala, F. D.; Morello, G.; Pompa, P.; Hytch, M.; Snoeck, E.; Fiore, A.; Franchini, I. R.; Nadasan, M.; Silvestre, A. F.; Chiodo, L.; Kudera, S.; Cingolani, R.; Krahne, R.; Manna, L. Synthesis and Micrometer-Scale Assembly of Colloidal CdSe/CdS Nanorods Prepared by a Seeded Growth Approach. *Nano Lett.* **2007**, *7*, 2942−2950.
(26) Christodoulou, S.; Vaccaro, G.; Pinchetti, V.; De Donato, F.; Grim, J. Q.; Casu, A.; Genovese, A.; Vicidomini, G.; Diaspro, A.; Brovelli, S.; Manna, L.; Moreels, I. Synthesis of Highly Luminescent Wurtzite CdSe/CdS Giant-Shell Nanocrystals Using a Fast Continuous Injection Route. *J. Mater. Chem. C* **2014**, *2*, 3439−3447.
(27) Mark, P. The Role of Chemisorption in Current Flow in Insulating CdS Crystals. *J. Phys. Chem. Solids* **1965**, *26*, 959−972.
(28) Vuylsteke, A. A.; Sihvonen, Y. T. Sulfur Vacancy Mechanism in Pure CdS. *Phys. Rev.* **1959**, *113*, 40−42.
(29) Chrysochoos, J. Recombination Luminescence Quenching of Nonstoichiometric CdS Clusters by ZnTPP. *J. Phys. Chem.* **1992**, *96*, 2868−2873.
(30) Lu, W.; Tokuhiro, Y.; Urnezu, I.; Sugimura, A.; Nagasaki, Y. Trap State Emission of Water-Soluble CdS Nanocrystals. *Phys. Status Solidi C* **2009**, *6*, 346−349.
(31) Zhao, P. Q.; Xiong, S. J.; Wu, X. L.; Chu, P. K. Photoluminescence Induced by Twinning Interface in CdS Nanocrystals. *Appl. Phys. Lett.* **2012**, *100*, 171911.
(32) Foussekis, M.; Baski, A. A.; Reshchikov, M. A. Photoadsorption and Photodesorption for GaN. *Appl. Phys. Lett.* **2009**, *94*, 162116.
(33) Gu, Y.; Lauhon, L. J. Space-Charge-Limited Current in Nanowires Depleted by Oxygen Adsorption. *Appl. Phys. Lett.* **2006**, *89*, 143102.
(34) Jasinski, P.; Suzuki, T.; Anderson, H. U. Nanocrystalline Undoped Ceria Oxygen Sensor. *Sens. Actuators, B* **2003**, *95*, 73−77.
(35) Smyntyna, V.; Gerasutenko, V.; Golovanov, V.; Kaciulis, S.; Mattogno, G.; Viticoli, S. Surface Spectroscopy Study of CdSe and CdS Thin-Film Oxygen Sensors. *Sens. Actuators, B* **1994**, *22*, 189−194.
(36) Reed, C. E.; Scott, C. G. Surface States on Single Crystals of Cadmium Sulphide. *Br. J. Appl. Phys.* **1964**, *15*, 1045−1050.
(37) Leatherdale, C. A.; Kagan, C. R.; Morgan, N. Y.; Empedocles, S. A.; Kastner, M. A.; Bawendi, M. G. Photoconductivity in CdSe Quantum Dot Solids. *Phys. Rev. B* **2000**, *62*, 2669−2680.
(38) Britnell, L.; Gorbachev, R. V.; Jalil, R.; Belle, B. D.; Schedin, F.; Katsnelson, M. I.; Eaves, L.; Morozov, S. V.; Mayorov, A. S.; Peres, N. M. R.; Castro Neto, A. H.; Leist, J.; Geim, A. K.; Ponomarenko, L. A.; Novoselov, K. S. Electron Tunneling through Ultrathin Boron Nitride Crystalline Barriers. *Nano Lett.* **2012**, *12*, 1707−1710.
(39) Simmons, J. G. Generalized Formula for the Electric Tunnel Effect between Similar Electrodes Separated by a Thin Insulating Film. *J. Appl. Phys.* **1963**, *34*, 1793−1803.
(40) Geyer, S.; Porter, V. J.; Halpert, J. E.; Mentzel, T. S.; Kastner, M. A.; Bawendi, M. G. Charge Transport in Mixed CdSe and CdTe Colloidal Nanocrystal Films. *Phys. Rev. B* **2010**, *82*, 155201.
(41) Meissner, D.; Lauermann, I.; Memming, R.; Kastening, B. Photoelectrochemistry of Cadmium Sulfide. 2. Influence of Surface-State Charging. *J. Phys. Chem.* **1988**, *92*, 3484−3488.
(42) Sze, S. M.; Ng, K. K. *Physics of Semiconductor Devices*, 3rd. ed.; Wiley-Interscience: Hoboken, NJ, 2006.
(43) Law, J. T. The Interaction of Oxygen with Clean Silicon Surfaces. *J. Phys. Chem. Solids* **1958**, *4*, 91−100.
(44) Melnick, D. A. Zinc Oxide Photoconduction, an Oxygen Adsorption Process. *J. Chem. Phys.* **1957**, *26*, 1136−1146.
(45) Eranna, G. *Metal Oxide Nanostructures as Gas Sensing Devices*, 1st ed.; Taylor & Francis Group: Boca Raton, 2011.
(46) Ting, Z.; Syed, M.; Nosang, V. M.; Marc, A. D. Recent Progress in Carbon Nanotube-Based Gas Sensors. *Nanotechnology* **2008**, *19*, 332001.
(47) Salehi-Khojin, A.; Lin, K. Y.; Field, C. R.; Masel, R. I. Nonthermal Current-Stimulated Desorption of Gases from Carbon Nanotubes. *Science* **2010**, *329*, 1327−1330.